Water Practice & Technology

IWA PUBLISHING

Water Practice & Technology Vol 19 No 8, 3272 doi: 10.2166/wpt.2024.198

Performance of bio-nest by modified basalt fiber carriers on the enhanced remediation of low-carbon and -nitrogen urban black-smelling water

Kai He [a,b,c], Jinlong Yuan[a,b,c], Xiaoyuan Qi[d], Haixia Yu[b], Haoxian Lu[e], Qidong Yin [b,c], Suo Zhang[f,*] and Bingjun Liu[b]

[a] Key Laboratory of Water Security Guarantee in Guangdong-Hong Kong-Marco Greater Bay Area of Ministry of Water Resources, Guangzhou 510611, China
[b] School of Civil Engineering, Sun Yat-Sen University, Zhuhai 519082, China
[c] Guangdong Provincial Key Laboratory for Marine Civil Engineering, Zhuhai 519082, China
[d] Zhuhai Water Resources Center, Zhuhai 519000, China
[e] Southern Marine Science and Engineering Guangdong Laboratory (Zhuhai), Zhuhai 519082, China
[f] Shanghai Municipal Engineering Design Institute (Group) Co., Ltd, Tianjin Branchi, Tianjin 300220, China
*Corresponding author. E-mail: zhangsuo@smedi.com

KH, 0000-0002-1041-0738; QY, 0000-0002-9063-5397

ABSTRACT

Biological contact oxidation reactors employing modified basalt fiber (MBF) were constructed to systematically investigate the impact of various hydraulic retention times (HRTs) and aeration durations on nitrogen and phosphorus removal in low carbon and polluted river water. The experimental findings underscored that configuring the HRT to 36 h and maintaining an aeration ratio of 1:2 yielded the most favorable outcomes for the removal of chemical oxygen demand, NH_4^+ -N, total nitrogen (TN), and TP from synthetic low carbon, source-polluted river water. Detailed microbial sequencing elucidated the predominant bacterial phylum within the MBF reactor, identified as Proteobacteria. The dominant genera encompassed *Pseudomonas*, *Aeromonas*, and *SM1A02*. This microbial composition, marked by a high abundance of denitrifying genera, corroborated the robust denitrification capacity exhibited by the MBF reactors. The orchestrated combination of optimal operational parameters and the prevalence of key microbial taxa substantiate the efficiency of MBF reactors in effectively mitigating nitrogen and phosphorus in low carbon source river water.

Key words: modified basalt fiber, biological contact oxidation, low C/N, urban river

HIGHLIGHTS

- A modified basalt fiber (MBF) filler was used with specific aeration and retention time for effective low C/N black-odor water treatment.
- About 68.52% of phosphorus removal in certain conditions was achieved.
- The MBF reactor hosts denitrification and nitrification bacteria, enhancing nitrogen removal processes.
- The MBF filler proves to be a reliable solution for low carbon water remediation.

GRAPHICAL ABSTRACT

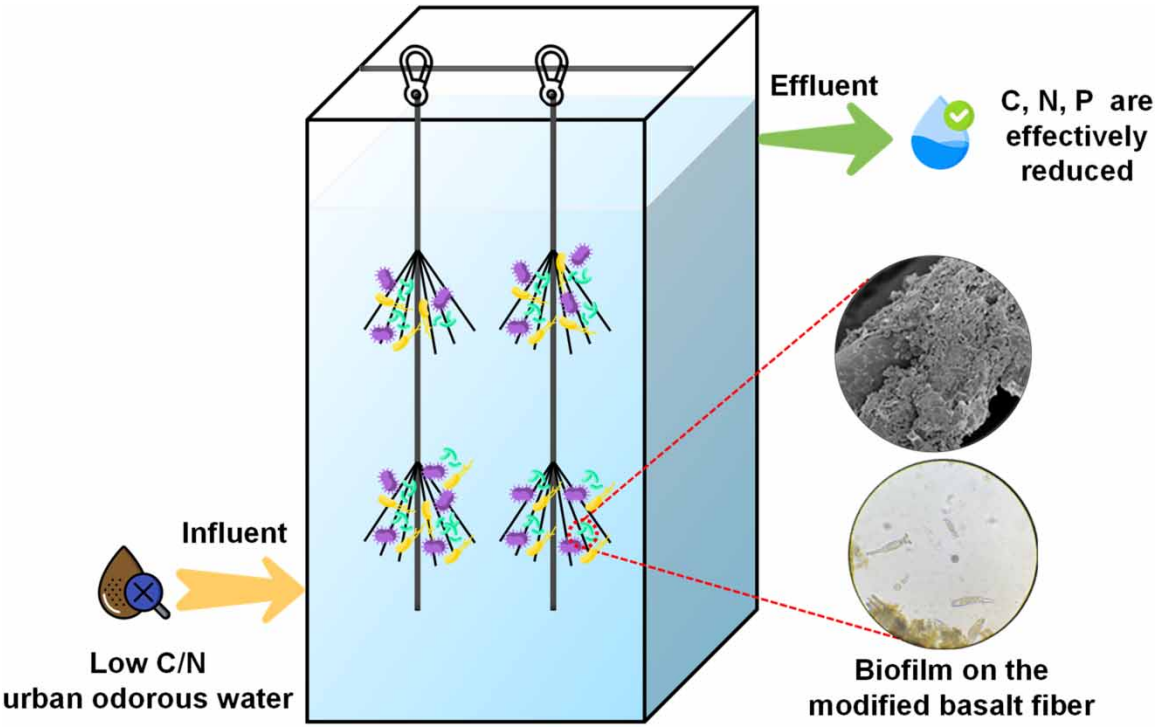

1. INTRODUCTION

Urban industrialization continually increases wastewater discharge, particularly in densely populated and developed cities where high nitrogen content is common in both domestic and industrial effluents. High nitrogen levels in aquatic environments lead to eutrophication and the deterioration of water quality (Zhang *et al.* 2022; He *et al.* 2023). Urban rivers in China typically exhibit low carbon-to-nitrogen (C/N) ratios and elevated total nitrogen (TN) concentrations, typically near 10 mg/L. These concentrations predominantly consist of nitrate nitrogen ($NO_3^- - N$) (Tu *et al.* 2019). As urban lifestyles evolve, nitrogen concentrations are suggested to keep increasing and further decreasing the C/N ratio (Tian & Yu 2020). However, optimal denitrification requires a C/N ratio between 6 and 11 and can operate minimally at 3.5–4.5 (Liu *et al.* 2019). Low C/N-ration conditions pose substantial challenges to denitrification processes (Zheng *et al.* 2023). Organic carbon deficiency necessitates the addition of external organic carbon sources, such as methanol and sodium acetate, to facilitate heterotrophic denitrification, transforming nitrate into dinitrogen. However, these conventional nitrogen removal methods are costly and inefficient (Ni *et al.* 2021; Zhai *et al.* 2022).

Attached growth processes, such as biofilm reactors, are gaining attention due to their sustainability, cost-effectiveness, and eco-friendly nature, offering an easily scalable and self-sufficient solution (Ni *et al.* 2021; Thuy *et al.* 2022). Nutrient concentration, influent water quality, and carrier nature are vital factors influencing biomass and the nutrient removal of biofilm reactors (Leyva-Diaz *et al.* 2020; Ouyang *et al.* 2023). Biofilm systems, leveraging the benefits of increased microorganism–wastewater contact, surpass suspended growth variants in terms of volumetric loads due to the extensive specific surface area of carriers and enhanced biomass retention (Roche *et al.* 2017; Gao *et al.* 2021). Among various carrier materials, modified basalt fiber (MBF) is emerging as a promising eco-friendly inorganic fiber option for wastewater treatments due to its substantial specific area, minimal hydraulic resistance, and excellent permeability (Liu *et al.* 2018). Notably, continuous MBF has been shown to outperform glass and polymeric fibers in terms of tensile strength and chemical stability, with studies indicating rapid microbial attachment and proliferation, thus affirming its potential as an effective biocarrier material (Ni *et al.* 2018).

The ability of MBF bioreactors to effectively remove nitrogen, particularly across diverse nitrogen concentrations, offers valuable guidance for bioreactor refinement. For example, the MBF carrier introduced in the reactor captured more versatile microorganisms and achieved a 85% chemical oxygen demand (COD) removal rate at low C/N. A review showed that with the introduction of MBF bio-carriers, the baffled anaerobic–aerobic

reactors exhibited TN removal efficiencies comparable to those of the anoxic/anoxic biological aerated filter (BAF) process, reaching 81% (Zhou *et al.* 2022; Cai *et al.* 2023). MBF-based bioreactors enhance the microbial community dynamics and functionality, leading to improved nitrification stability and denitrification efficacy (Ni *et al.* 2018). For example, the reduction of *Saccharibacteria* and a concomitant increase in *Betaproteobacteria* from the external to internal regions of the bio-nest were observed, highlighting the inherent aerobic/anaerobic interplay (Gao *et al.* 2021). The multifaceted construct of MBF bioreactors fosters an enriched bacterial biodiversity (Zhang *et al.* 2019a). MBF has a water contact angle of 61.64 and is spontaneously hydrophilic. Therefore, bacteria adhered more strongly to the surface of MBF in the initial stage, and microscopic observation showed that MBF was tightly adhered to the surface of the MBF biocarrier by a large number of bacteria (Zhang *et al.* 2019b). When juxtaposed with conventional biofilms, MBF-based bio-nests manifest pronounced heterogeneity, especially in terms of oxygen gradients and bacterial community spatial distribution. Crucially, the optimized mass transport within bio-nests facilitates superior biomass immobilization, as evidenced in studies on calcium-MBF bio-carriers (Gao *et al.* 2021).

Despite the promising advances, research into the roles of MBF as bio-carriers, particularly for urban river remediation, remains nascent. It is postulated that MBF might amplify microbial adhesion and biological degradation, thereby elevating remediation efficiency. Consequently, this study aims to examine the impact of carriers on water treatment and microbial enrichment. We meticulously evaluated these carriers' long-term water processing efficacy of across varying nitrogen concentrations. In addition, employing high-throughput 16S ribosomal ribonucleic acid (rRNA) gene sequencing, we deciphered the bacterial community residing on these carriers. Our endeavor aims to provide deeper insights into the operational nuances and nitrogen elimination capabilities of bioreactors that employ ultrafine fiber carriers.

2. MATERIALS AND METHODS

2.1. Experimental setup

Two MBF reactors were set up and operated to simulate urban river remediation. The reactors measured were 40 cm in length, 40 cm in width, and 70 cm in height and constructed from acrylic glass plates. The effective volume of the reactors was approximately 85 L, of which 70 L was designed for the water phase in urban rivers, and the remaining 15 L represents riverbed sediment. MBF was applied as a biocarrier and as described in previous studies (Ni *et al.* 2023). The scheme of the MBF reactor is shown in Figure 1. Each MBF bundle had a diameter of 14 cm, and within the reactor, four bundles (comprising two strings) of MBF bio-carriers were suspended (Table S1). These MBF bundles were securely anchored at both the top and bottom. There is a horizontal gap of 15 cm separating the two bundles of MBF. The MBF reactor experiments were conducted indoors without direct sunlight therefore, the reactors were not covered to prevent the potential effects of light.

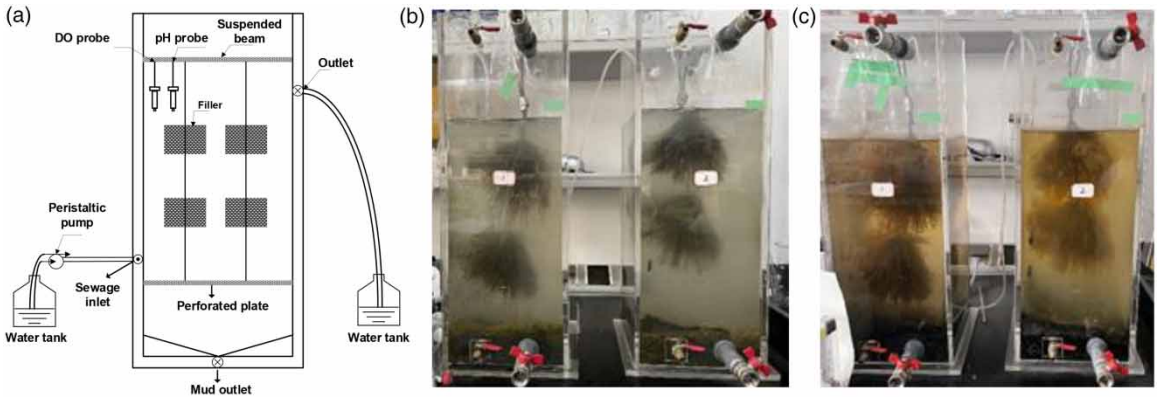

Figure 1 | Scheme of the MBF reactor. (a) Schematic diagram of the reactor, (b) startup of MBF reactors, and (c) biofilm formation in MBF reactors.

2.2. Synthetic urban water and sampling

The sediment was sourced from the riverbed sediment of an urban river in Xiangzhou, Zhuhai, Guangdong, China. Synthetic urban water was used as feed water. The concentrations of components in synthetic urban

water were determined based on the previous studies on water quality monitoring results of urban polluted rivers in Guangdong provincial surveys (Gao *et al.* 2023). Glucose ($C_6H_{12}O_6$) is used as a carbon source. TN concentration was maintained at 20 mg/L. The C/N ratio was maintained at 5. Particularly, the concentrations of ammonium and nitrate in urban rivers located in Guangdong varied (Xuan *et al.* 2020). Therefore, two concentration ratios of NH_4^+–N to NO_3^-–N were set at 1:1 (MBF-1) and 1:3 (MBF-2) for two MBF reactors, respectively. Table S2 shows the concentrations of components in the two types of synthetic urban water.

Furthermore, an electromagnetic oxygenation pump was employed for aeration and oxygen supply. Both reactors initially had a 72-h hydraulic retention time (HRT) and a 2:1 aeration ratio. To determine and control the HRT, the working volume of the reactor is measured and divided by the system flow rate. By carefully controlling the outlet flow rate, the HRT can be precisely adjusted. The working volume of the reactor is 70 L, and if the HRT is set to 72 h, the flow rate of the control system is 0.98 L/h. During the reactor operation, HRTs and aeration duration ratios were adjusted based on the performance of pollutant removal. Aeration control is performed in units of 24 h a day; the aeration ratio indicates the ratio of aeration to unaerated time, and the aeration time indicates the total aeration time of the day. For example, if the aeration ratio is 2:1, the aeration time would be two-thirds of 24 h, equating to 16 h/day. Detailed operation parameters are shown in Table 1. After changing HRT or aeration duration, each stage had a 10-day stabilization period. The 10-day experimental period was chosen based on empirical evidence, literature support, preliminary findings, and practical considerations (Duan & Kravaris 2017; Lu *et al.* 2020). It allows for a robust assessment of throughput stability while acknowledging the complexities of microbial community dynamics. The reactors consistently operated with a dissolved oxygen (DO) of 2–3 mg/L, a pH of 6.9–7.5, and a room temperature of 20–25 °C. Effluent water samples were collected and measured daily.

Table 1 | Detailed operation parameters of two MBF reactors

Reactor	Date	HRT (h)	Aeration ratio (with aeration/without aeration)	Aeration time (h/day)	DO (mg/L)	Microbial sampling site
MBF-1	Day 1–10	72	2:1	16	2–3	ST.2.1
	Day 11–20	72	1:2	8	2–3	ST.1.2
	Day 21–30	36	1:2	8	2–3	TS.1.2
	Day 31–40	24	1:2	8	2–3	TF.1.2
MBF-2	Day 1–10	72	2:1	16	2–3	A1
	Day 11–20	36	2:1	16	2–3	A2
	Day 21–30	36	1:2	8	2–3	A3

2.3. Analytical method

2.3.1. Chemical analysis

The concentration of COD was measured using the standard digestion spectrophotometric methods. NH_4^+–N concentration was measured employing Nessler's reagent spectrophotometry. Ultraviolet spectrophotometry combined with an alkaline potassium persulfate digestion was used to determine the TN levels. The total phosphorus (TP) concentration was assessed through the digestion-ascorbic acid technique. Detailed experimental methods could be referred to the 'Water Analysis Handbook' by Hach (Hach 2016).

2.3.2. Morphological analysis and material characteristics

To systematically investigate and compare alterations in the surface morphology and roughness of MBF, MBF specimens were affixed directly onto a conductive adhesive substrate. Subsequently, a 45-s gold sputtering treatment at 10 mA was administered using the Quorum SC7620 sputtering coater. The surface characteristics of these fibers were subsequently captured through imaging utilizing a TESCAN MIRA LMS scanning electron microscope (SEM), manufactured by Oxford Instruments in the United Kingdom. Following the acquisition of surface morphology images for MBF, an in-depth analysis of the elemental composition was conducted employing energy spectrum line scanning techniques. This analysis was executed utilizing the TESCAN MIRA LMS SEM, which was equipped with an X-ray energy dispersive spectrometer (SEM-EDS).

2.3.3. Microbial community analysis

16S rRNA high-throughput sequencing was applied to determine the microbial diversity and community structure. Microbial samples adhered to the MBF fillers were collected at the end of each stage (Table 1). DNA was extracted using the ALFA-SEQ Advanced Soil DNA Kit (mCHIP BioTech CO., LTD, China). The integrity, purity, and concentration of the extracted DNA were verified using 1% agarose gel electrophoresis and the Thermo NanoDrop One spectrophotometer. The V3–V4 variable regions of the bacterial 16S rRNA gene were polymerase chain reaction (PCR)-amplified with primers 338F (5′-ACTCCTACGGGGAGGCAGCA-3′) and 806F (5′-GGACTACHVGGGGTWTCTAAT-3′). The PCR comprised 25 μL of Premix Taq (2×), 1 μL each of both the forward and reverse primers (10 μM), 50 ng of DNA, and nuclease-free water added to make up a total volume of 50 μL (Chen *et al.* 2018). The PCR protocol entailed an initial denaturation at 94 °C for 5 min, followed by 30 cycles of denaturation at 94 °C for 30 s, annealing at 52 °C for 30 s, and extension at 72 °C for 30 s, culminating in a final extension at 72 °C for 10 min. The reaction was then stored at 4 °C. Post-amplification, PCR products were pooled and purified utilizing the E.Z.N.A.® Gel Extraction Kit, and a sequencing library was constructed as per the NEBNext® Ultra™ DNA Library Prep Kit for Illumina® protocol (Amir *et al.* 2017). Sequencing was executed on the Illumina Nova 6000 platform. Operational taxonomic units (OTUs) with over 97% similarity were clustered using the UPARSE software (Edgar 2013). Redundancy analysis (RDA) was performed using the Microeco package by R 4.2.2 and RStudio to characterize the microbial community composition of the two groups as affected by water quality.

3. RESULTS AND DISCUSSION

3.1. Removal performance of COD

Figure 2(a) delineates the COD removal efficiency performance of MBF-1 within defined operational parameters. Under an HRT of 72 h and an aeration time ratio of 2:1, the reactor exhibited an average COD removal rate of

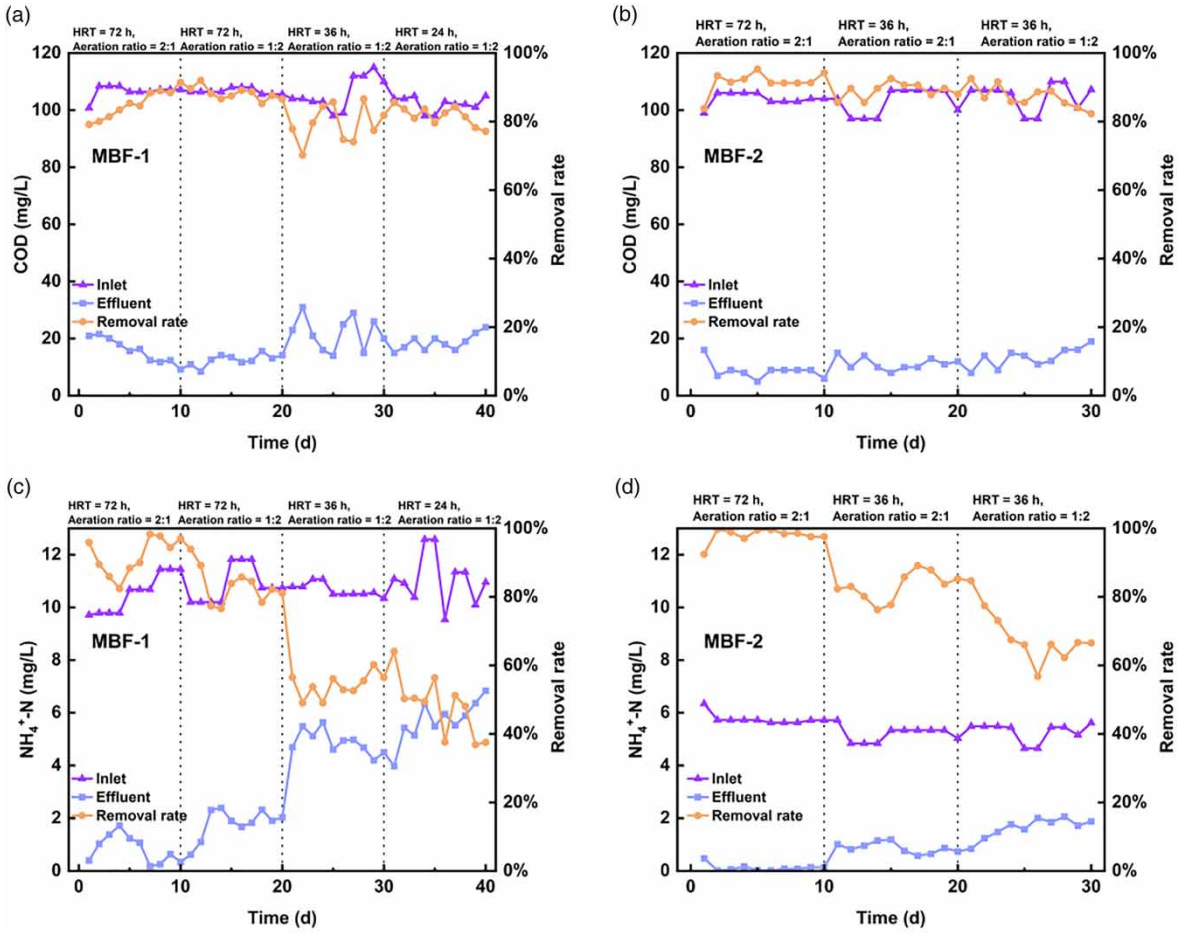

Figure 2 | Influent and effluent concentrations of (a) COD in MBF-1, (b) COD in MBF-2, (c) NH_4^+ in MBF-1, and (d) NH_4^+ in MBF-2.

86.42%. Notably, a reduction in aeration time to 8 h led to a modest improvement in the COD removal rate, reaching 88.12%. The facilitated oxygen supply enabled microorganisms to efficiently utilize available oxygen, catalyzing the metabolization of organic pollutants and promoting microbial growth and proliferation (Saini *et al.* 2023). Moreover, the prolonged HRT (6 h) fostered an extended interaction between microorganisms and organic pollutants, thereby enhancing adsorption and degradation processes (Ahmad *et al.* 2017). Maintaining an aeration ratio of 1:2 preserved stable COD removal, suggesting that alterations in aeration time did not significantly impact system performance. However, a reduction in HRT from 72 to 36 h increased COD effluent concentration, leading to a slight drop in the average COD removal rate to 79.25%. Further shortening the HRT to 24 h maintained a consistent COD removal level. In essence, the presence of the MBF filler substantially retained biomass within the system. Despite HRT reductions, a sufficient population of heterotrophic bacteria adhered to the carrier, ensuring the degradation of organic matter. Consequently, under varied conditions, the system consistently achieved an average COD removal rate of approximately 80%.

Figure 2(b) illustrates the COD removal efficiency performance of MBF-2. A decrease in both HRT and aeration duration resulted in a slight reduction in the COD removal rate. However, this decline was not pronounced, and the system consistently maintained a high and relatively stable COD removal rate. Specifically, at an HRT of 72 h with aeration at a 2:1 ratio, the MBF system demonstrated the highest average COD removal rate at 91.58%. Shortening the HRT led to a reduction in the average COD removal rate to 88.99%. Furthermore, when the aeration duration was shortened to 8 h, the average COD removal rate reached 87.18%. The packing within the system facilitated biomass enrichment, resulting in higher biomass retention within the reactor. Consequently, under all three conditions, the average COD removal rate exceeded 85%, indicating the efficacy of MBF-2 in organic matter removal.

3.2. Changes of ammonia nitrogen during operation

As illustrated by the data in Figure 2(c), a conspicuous elevation in NH_4^+–N effluent concentrations was observed in the MBF-1 reactor when both HRT and aeration duration were reduced. Specifically, under an HRT of 72 h, the recorded average effluent concentrations were 0.8 and 1.92 mg/L for aeration-to-discontinued aeration ratios of 2:1 and 1:2, respectively. These patterns suggest that prolonged aerobic conditions stimulate the growth and metabolism of nitrifying bacteria, thereby enhancing nitrification efficiencies (Mariane de Morais *et al.* 2020; Nemeth *et al.* 2023). Under optimal conditions, removal rates surged beyond 82%. However, a reduction in the HRT to 36 h triggered an increase in organic loading, promoting the proliferation of heterotrophic bacteria. This, coupled with diminished contact time with pollutants due to the shortened HRT, disadvantaged autotrophic nitrifying bacteria. Consequently, there was a notable increase in effluent NH_4^+–N concentrations, leading to dwindling removal rates, which reached 54.21 and 48.19% for HRTs of 36 and 24 h, respectively.

Figure 2(d) underscores the detrimental impact of the reduced HRT and aeration duration on nitrification efficacy in MBF-2. Under an HRT of 72 h and an aeration ratio of 2:1, MBF-2 demonstrated commendable NH_4^+–N removal rates, peaking at 97.93%, with effluent concentrations oscillating between 0.14 and 0.48 mg/L. However, a decrease in the HRT to 36 h significantly diminished the interaction time between the influent substrate and microbes. This, coupled with an augmented influent flow, potentially compromised biofilm integrity and depleted nitrifying bacteria populations, resulting in a decline in the removal rate to 83.13%. Further reducing the aeration duration to 8 h led to a progressive drop in removal rates, reaching 68.70%. The diminishing trend in the NH_4^+–N removal rate became evident with the shortened HRT and the aeration time.

Comparatively, while both reactors exhibited impressive NH_4^+–N removal rates under optimal conditions, MBF-2 displayed better removal rates. The performance of MBF-1 showed a more pronounced decline with reduced HRT and aeration duration compared to MBF-2. This suggests that MBF-2 may have a relatively more stable performance under varied operational conditions. The differing NH_4^+–N:NO_3^- ratios between MBF-1 and MBF-2 could be contributing to these observed variations in performance.

3.3. TN removal in MBF reactors

As depicted in Figure 3(a), in MBF-1, despite the slight increase of NH_4^+–N, a notable increase in the average TN removal rate, progressing from 39.07 to 61.94%, was observed by maintaining a consistent HRT of 72 h while adjusting the aeration-to-discontinued aeration time ratio from 2:1 to 1:2. The efficacy of biological denitrification heavily relies on the symbiotic interplay of nitrification and denitrification reactions. These results suggest that TN removal was predominantly steered by microbial denitrification. In anaerobic settings, denitrifying bacteria

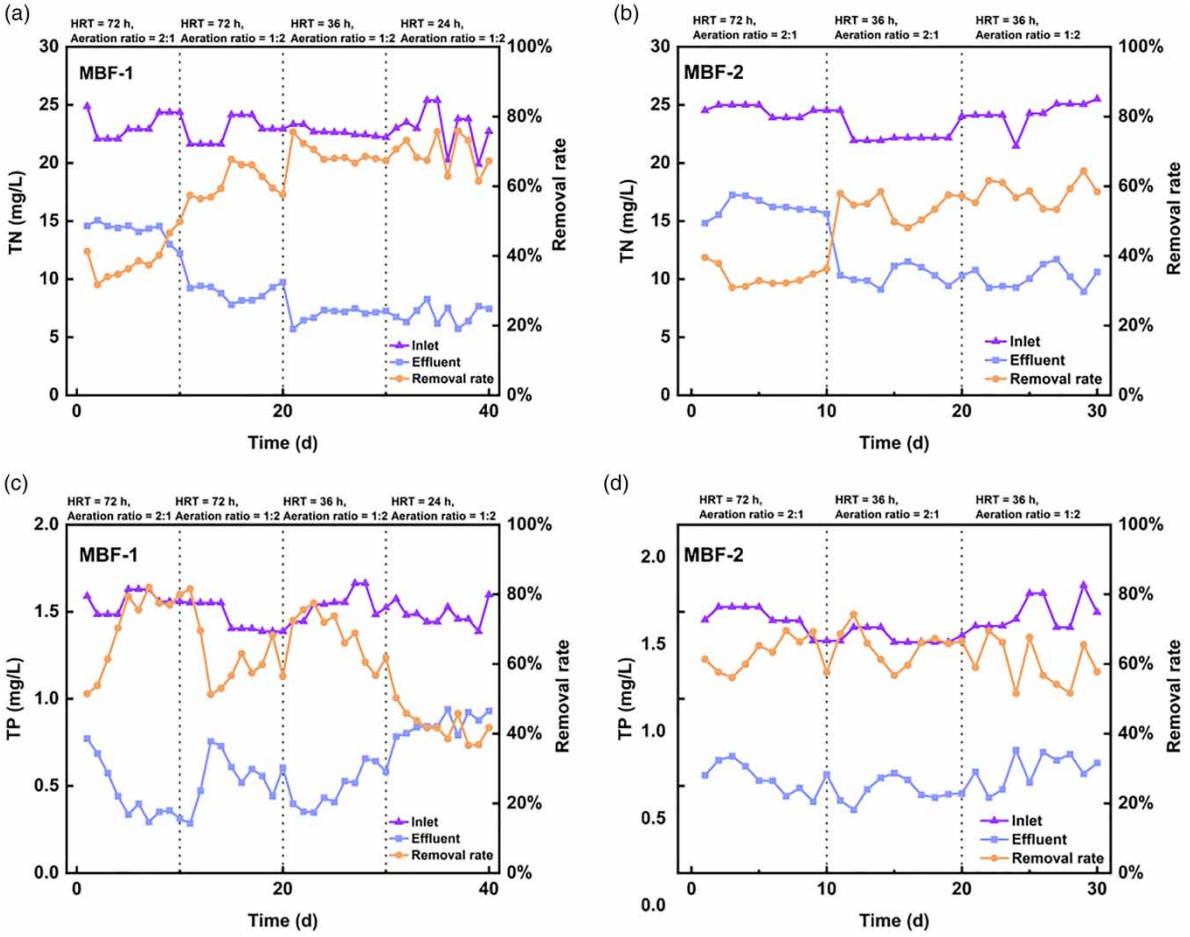

Figure 3 | Influent and effluent concentrations of (a) TN in MBF-1, (b) TN in MBF-2, (c) TP in MBF-1, and (d) TP in MBF-2.

leverage organic content to catalyze redox reactions, converting $NO_2^- - N$ and $NO_3^- - N$ into N_2, thereby affecting nitrogen elimination (Li *et al.* 2021). The 2:1 aeration-to-discontinued aeration time ratio, owing to its prolonged aerobic phase, proves unfavorable for the growth and persistence of denitrifying bacteria. This limitation curtails the denitrification rate, subsequently affecting TN removal efficiency. On the other hand, upon stabilizing the aeration-to-discontinued aeration ratio while varying the HRT from 72 h to 36 and 24 h, TN removal rates in MBF-1 were documented as 61.94, 69.29, and 69.58%, respectively. Therefore, shortening HRT to 24 h did not affect the overall TN removal rate.

In MBF-2, reducing the HRT from 72 to 36 h enhances the mean TN removal rate from 34.96 to 54.23% (Figure 3(b)). The diminished HRT intensifies the organic burden within the reactor, fostering the proliferation of heterotrophic denitrifying bacteria and thereby optimizing nitrogen removal (Niu *et al.* 2023). Maintaining the HRT at 36 h and adjusting the aeration-to-discontinued aeration time ratio from 2:1 to 1:2 induce a nearly 4% increase in the mean TN removal rate, accompanied by minimal deviations in the effluent concentration. Comparatively, the TN removal rate of MBF-2 was relatively lower than that of MBF-1, in contrast to $NH_4^+ - N$ removal, where MBF-2 exhibited superior removal performance. This result might be because the denitrification activity of MBF-2 was lower than that of MBF-1, while MBF-2 exhibited higher nitrification activity.

3.4. TP removal in MBF reactors

The removal rate of TP in MBF-1 exhibited an initial increase followed by a decrease with the extension of the HRT (Figure 3(c)). The best TP removal rate was observed when the HRT was 72 h and the aeration ratio was 2:1 (day 1–day 10), with the TP removal rate reaching almost 80% on day 10. Shifting the aeration rate from 2:1 to 1:2 led to a decrease in the TP removal rate from 73.52 to 59.44%. This significant decrease suggests that the TP removal activity benefited from extended aerobic stages. On the one hand, lower DO concentrations can compromise the activity of phosphorus-aggregating bacteria (Kim *et al.* 2003; Gong *et al.* 2023). On the other hand,

longer aerobic periods might bolster the ability of polyphosphorus bacteria to uptake and store phosphates. With a consistent aeration ratio, shortening the HRT from 72 h to 36 and 24 h resulted in a continuous decrease in the TP removal rate from 68.52 to 42.25%. This could be attributed to the short HRT hindering the interaction between microorganisms and substrates, as mentioned earlier. The short HRT provided a limited duration of time for polyphosphorus bacteria to absorb phosphate (Chen *et al.* 2022).

Figure 3(d) shows the TP removal variations in MBF-2. The manipulation of HRT and aeration duration did not significantly impact the average TP removal rate. However, the stability of phosphorus removal was profoundly influenced by variations in aeration duration. Under the conditions of a 72-h HRT and a 2:1 aeration ratio, the average TP removal rate in MBF-2 was recorded as 63.02%. Maintaining the HRT and reducing the aeration ratio to 1:2 resulted in a decline in the TP removal rate to 59.99%, accompanied by greater fluctuations in the removal curve. One plausible explanation is that the 2:1 aeration ratio was adequate for polyphosphorus bacteria to conclude the anaerobic phosphorus release process. Further reductions in aeration time impeded the aerobic phosphorus absorption process, thereby diminishing the stability of phosphorus removal.

3.5. Morphology of MBF and growth of biomass

The hydrophilicity or hydrophobicity of a material significantly influences the propensity of microorganisms to adhere to it. A critical parameter in determining the hydrophilicity or hydrophobicity of biofilm carriers is the water contact angle (Al-Amshawee *et al.* 2021). It is noted that microorganisms tend to selectively colonize surfaces of carriers exhibiting hydrophilicity, thereby enhancing the likelihood of biofilm formation. According to measurements obtained with a contact angle meter, the contact angle of MBF was determined to be 61.5°. Materials with a contact angle exceeding 90° are classified as hydrophobic, while those with angles below 90° are considered hydrophilic (Ni *et al.* 2022). The magnitude of the angle is inversely proportional to the degree of hydrophilicity. Therefore, the MBF utilized in this study possessed pronounced hydrophilicity, implying a propensity for dispersion in water. This characteristic suggests that MBF was conducive to microbial adhesion and subsequent biofilm development.

The microscopic morphology and elemental composition of MBF are meticulously illustrated in Figure S1 and Table S3. The results of SEM-EDS line spectra revealed that MBF primarily consists of inorganic materials, encompassing elements such as Si, Ti, Al, Na, Ca, K, Mg, O, and Fe, with Si and O being the predominant constituents. The diameter of MBF filaments was approximately 12 μm. Notably, there was a conspicuous increase in surface roughness, which was characterized by the presence of pits and irregular protrusions. Adhering to the fiber filament surfaces are fine granular substances. These morphological attributes significantly amplify the likelihood of interactions between microorganisms and the fiber surface, thereby facilitating microbial adhesion (Kalia *et al.* 2013). Furthermore, the amplified specific surface area of the material enhances the potential for microbial attachment.

As depicted in Figure 4, the basalt fibers are enveloped by a dense layer of microorganisms. The SEM results further reveal the close attachment of microorganisms to the MBF fibers, forming intricate and uneven layers. The spatial arrangement of basalt fibers, intricately interwoven with the biofilm, optimizes the transfer of nutrients from wastewater and facilitates the circulation of DO throughout the biofilm (Xia *et al.* 2015). Consequently, the matrix of the basalt filler may establish aerobic, anaerobic, and anaerobic zones, fostering diverse microenvironments. These varied environments create multiple niches for a spectrum of microbial communities, promoting the growth and proliferation of different functional microorganisms. The inherent diversity within the biofilm enables microorganisms to synergistically collaborate, enhancing pollutant removal with a potent synergistic effect (Zhang *et al.* 2018).

Upon concluding the initial phase for both reactors, fiber samples were extracted for a detailed examination of the biophase using an optical microscope. The graphical representation emphasizes a consistent distribution of yellow-brown activated sludge over the basalt fiber filaments. The manifested biofilm exhibits a dense architecture, with the sludge flocs remaining undisturbed – displaying neither disintegration nor expansion. With the gradual operation of the reactors, an array of microorganisms, including rotifers, bellworms, and schizothoracines, began to flourish, suggesting a diverse and healthy ecosystem within the reactors.

3.6. Microbial community analysis

The 16S rRNA high-throughput sequencing revealed a total of 642,399 reads across all samples, with an average read number of 9,177 and coverage indices exceeding 99.9%. The microbial α-diversity indices are summarized in Table 2. The Shannon and Simpson indices, employed to assess microbial diversity, exhibit higher values

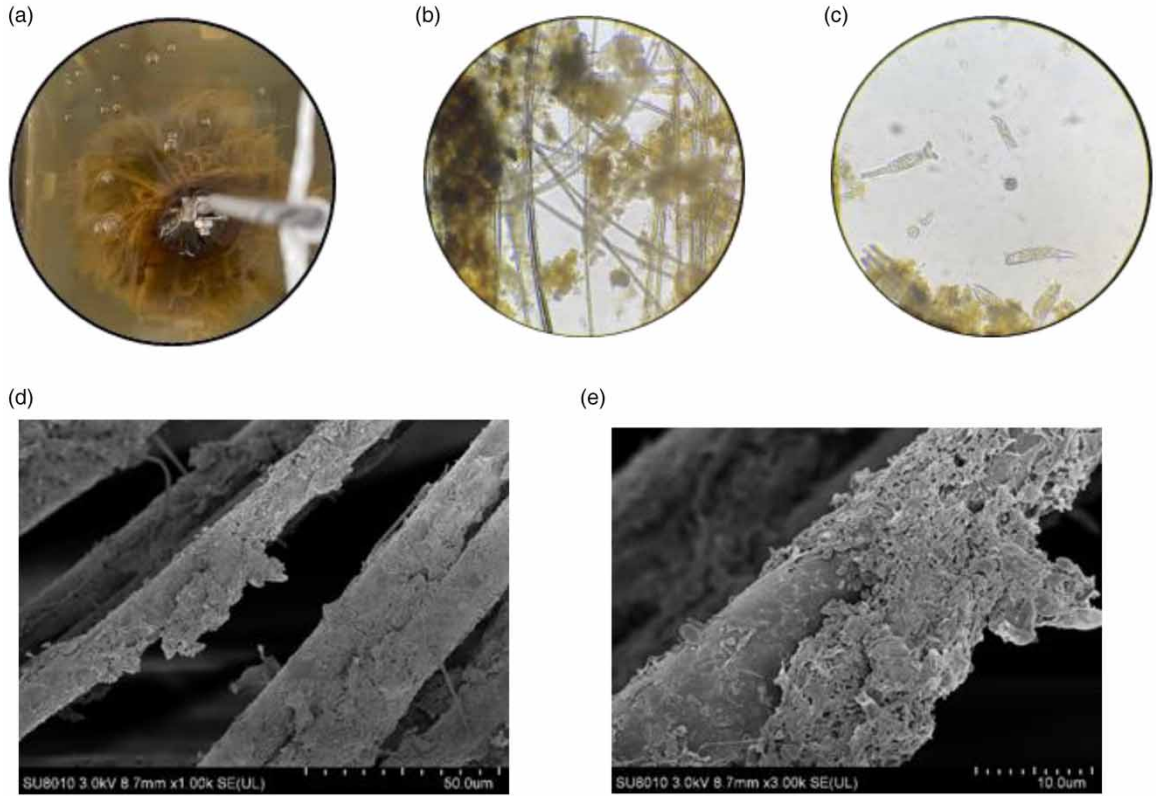

Figure 4 | Biofilm growth in MBF reactors. (a) Biofilm attached to the MBF, (b) biofilm structure of the MBF filament by microscopy, (c) protozoa are found in the reactors, (d) SEM images of the MBF after biofilm attachment (50 μm), and (e) SEM images of the MBF after biofilm attachment (10 μm).

Table 2 | Statistics of the α-diversity index of the bacterial community in reactors

Sample ID	Reactor	HRT (h)	Aeration ratio	Reads	OTUs	Shannon	Simpson	Chao1	Coverage (%)
ST.2.1	MBF-1	72	2:1	84,116	758	3.88	0.07	778.89	99.90
ST.1.2	MBF-1	72	1:2	84,820	876	4.21	0.05	898.98	99.90
TS.1.2	MBF-1	36	1:2	99,451	831	3.73	0.10	862.69	99.91
TF.1.2	MBF-1	24	1:2	93,607	768	3.47	0.14	806.68	99.90
A1	MBF-2	72	2:1	98,135	776	3.83	0.07	797.85	99.92
A2	MBF-2	36	2:1	89,602	934	3.77	0.10	939.03	99.95
A3	MBF-2	36	1:2	92,668	840	3.55	0.08	853.45	99.92

corresponding to increased species diversity within the community (Kim *et al.* 2017). In this study, both the highest Shannon indices and the lowest Simpson indices were observed in samples with an HRT of 72 h, suggesting that longer HRT favored microbial diversity (Liu *et al.* 2015). In addition, since light is one of the factors that may also affect the microbial community structure, the effects of light on microbial communities should be considered in subsequent studies. Figure 5(a) illustrates the phylum-level microbial composition, presenting the top 15 relative abundances of samples under each condition for the two reactors. Notably, Proteobacteria, Bacteroidetes, Actinobacteria, and Planctomycetes constitute substantial proportions in terms of relative abundance. The prevailing phylum across all samples was Proteobacteria, with relative abundance percentages ranging from 58.6 to 78.9%. Proteobacteria, as the most expansive bacterial phylum, exclusively comprises Gram-negative bacteria (Shang *et al.* 2022). Renowned for its high environmental adaptability, this phylum encompasses diverse metabolic flora capable of organic matter degradation, denitrification, and phosphorus removal (Siyu *et al.* 2021). Actinobacteria, recognized for its prowess in decomposing proteins and organic matter, harbors a significant

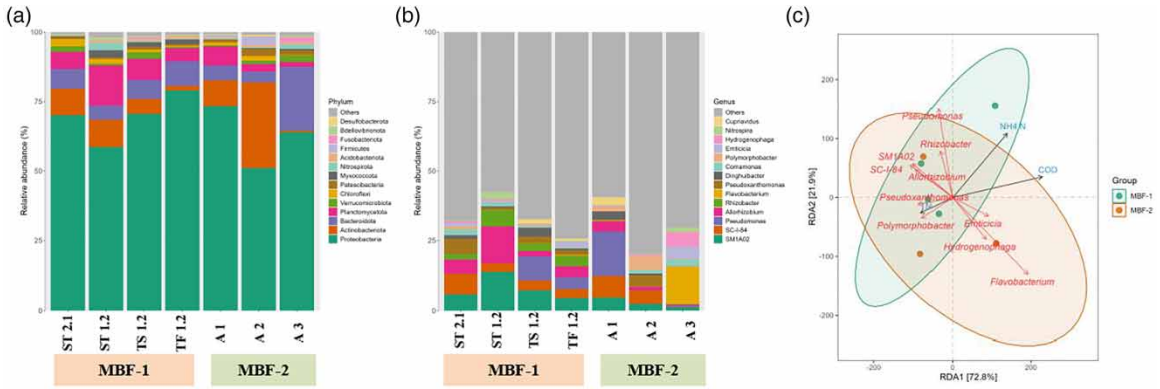

Figure 5 | Microbial community structure at (a) phylum level, (b) genus level, and (c) RDA analysis of the microbial community.

amount of heterotrophic nitrifying bacteria, playing a pivotal role in the degradation of recalcitrant substances like cellulose and chitin (Duan *et al.* 2022). In the A2 sample (MBF-2 with the HRT of 36 h and the aeration ratio of 2:1), its relative abundance reached 30.9%. Conversely, in the A3 sample (MBF-2 with the HRT of 36 h and the aeration ratio of 1:2), Bacteroidetes emerged as the second-most dominant phylum (23.0%). Functioning primarily in anaerobic conditions, Bacteroidetes excels in the degradation of organic matter, particularly macromolecular organic compounds such as proteins and sugars (Che *et al.* 2021).

Figure 5(b) shows the dominant microbial composition at the genus level for each sample. The predominant genera observed across the groups encompassed *Pseudomonas*, *Aeromonas*, *SM1A02*, *SC-I-18*, and so on. Key denitrifying bacteria genera identified from the samples included *SM1A02*, *Dechloromonas*, *Flavobacterium*, *Hyphomicrobium*, *Hydrogenophaga*, *Rhodobacter*, *Pseudomonas*, and *Aeromonas*. In addition, nitrifying bacteria, *Nitrospira*, was also enriched in the reactors. *Rhodobacter*, notably, functions as an aerobic denitrifying bacterium, facilitating the simultaneous nitrification–denitrification process. *Hydrogenophaga*, an autotrophic bacterium, actively participates in denitrification. *SM1A02*, frequently encountered in water treatment, exhibits anaerobic ammonia oxidation functionality, enabling the conversion of NH_4^+–N to N_2, thus facilitating denitrification (Hoshino *et al.* 2005). *Aeromonas*, known for its resistance to both acid and alkali and remarkable temperature adaptability, demonstrates the capability to degrade polycyclic aromatic hydrocarbons. Recent research reported the potential denitrification characteristics of *Aeromonas*, contributing to nitrate nitrogen reduction for TN removal (Tan *et al.* 2021). Samples TF.1.2 and A3, which showcased optimal nitrogen removal, also exhibited the highest proportions of denitrifying bacteria genera at 52.98 and 47.01%, respectively. This implies that the MBF system performs optimally in nitrogen removal under these specific conditions.

RDA1 accounted for 72.8% of the dataset, while RDA2 explained 21.9%; together, they comprehensively covered 94.7% of the data. This comprehensive explanation contributed to a clear demarcation between the two groups. The microbial composition of MBF-1 exhibited a significant correlation with NH_4^+–N and TN. While *Pseudomonas*, *Rhizobacter*, and *Allorhizobium* in the MBF-2 microbial community were positively correlated with NH_4^+–N and TN, *Flavobacterium* and *Hydrogenophaga* were positively correlated with COD.

4. CONCLUSION

This study underscores the efficacy of MBF carriers in enhancing the remediation of low carbon and nitrogen urban black-smelling water through biological contact oxidation reactors. Experimental findings demonstrated that an HRT of 36 h and an aeration ratio of 1:2 are optimal for removing COD, NH_4^+–N, TN, and TP. MBF-2 reactors maintained both high COD (>85%) and NH_4^+–N removal (97.93%) rates under optimal conditions. TN removal, driven by microbial denitrification, was the most efficient in the MBF-1 reactor. The hydrophilicity and rough surface morphology of MBF significantly facilitated microbial adhesion and biofilm formation. High-throughput 16S rRNA sequencing revealed diverse microbial communities, with the highest diversity under longer HRT conditions. MBF reactors predominantly hosted Proteobacteria, with a high abundance of denitrifying genera such as *Pseudomonas*, *Aeromonas*, and *SM1A02*, underscoring their robust denitrification capacity. Overall, MBF bioreactors present a promising solution for urban river water treatment.

ACKNOWLEDGEMENTS

This work was supported by the Open Research Fund of the Key Laboratory of Water Security Guarantee in Guangdong-Hong Kong-Marco Greater Bay Area of Ministry of Water Resources (Grant No. WSGBA-KJ202303), Foshan Shunde District Core Technology Breakthrough Project (2230218004273), 2022 Zhuhai Social Development Science and Technology Program Project (2220004000355), and Guangdong Basic and Applied Basic Research Foundation (2023B1515040028).

DATA AVAILABILITY STATEMENT

All relevant data are included in the paper or its Supplementary Information.

CONFLICT OF INTEREST

The authors declare there is no conflict.

REFERENCES

Ahmad, M., Liu, S., Mahmood, N., Mahmood, A., Ali, M., Zheng, M. & Ni, J. 2017 Synergic adsorption-biodegradation by an advanced carrier for enhanced removal of high-strength nitrogen and refractory organics. *ACS Applied Materials & Interfaces* **9**(15), 13188–13200. https://doi.org/10.1021/acsami.7b01251.

Al-Amshawee, S., Yunus, M. Y. B. M., Lynam, J. G., Lee, W. H., Dai, F. & Dakhil, I. H. 2021 Roughness and wettability of biofilm carriers: A systematic review. *Environmental Technology & Innovation* **21**. https://doi.org/10.1016/j.eti.2020.101233.

Amir, A., McDonald, D., Navas-Molina, J.A., Kopylova, E., Morton, J.T., Xu, Z.Z., Kightley, E.P., Thompson, L.R., Hyde, E.R., Gonzalez, A. & Knight, R. 2017 Deblur rapidly resolves single-nucleotide community sequence patterns. *Msystems* **2**(2). https://doi.org/10.1128/mSystems.00191-16.

Cai, H.-Y., Wu, Q.-Y., Ouyang, W.-Y., Hu, H.-Y. & Wang, W.-L. 2023 Efficient removal of electroneutral carbonyls by combined vacuum–UV oxidation and anion-exchange resin adsorption: Mechanism, model simulation, and optimization. *Water Research* **243**, 120435. https://doi.org/https://doi.org/10.1016/j.watres.2023.120435.

Che, J., Bai, Y., Li, X., Ye, J., Liao, H., Cui, P., Yu, Z. & Zhou, S. 2021 Linking microbial community structure with molecular composition of dissolved organic matter during an industrial-scale composting. *Journal of Hazardous Materials* **405**. https://doi.org/10.1016/j.jhazmat.2020.124281.

Chen, S., Zhou, Y., Chen, Y. & Gu, J. 2018 Fastp: An ultra-fast all-in-one FASTQ preprocessor. *Bioinformatics* **34**(17), 884–890. https://doi.org/10.1093/bioinformatics/bty560.

Chen, Y., Li, L., Zhang, Y., Pan, Y., Ni, M., Yang, W. & Huang, Y. 2022 Phosphorus absorption and release in biofilm sequencing batch reactor: The combined action of cells and extracellular polymeric substances and the characteristics of polymer metabolism. *Journal of Water Process Engineering* **49**. https://doi.org/10.1016/j.jwpe.2022.102979.

Duan, Z. & Kravaris, C. 2017 Robust stabilization of a two-stage anaerobic bioreactor system. In *2017 IEEE 56th Annual Conference on Decision and Control, CDC*, pp. 2083–2088.

Duan, S., Zhang, Y. & Zheng, S. 2022 Heterotrophic nitrifying bacteria in wastewater biological nitrogen removal systems: A review. *Critical Reviews in Environmental Science and Technology* **52**(13), 2302–2338. https://doi.org/10.1080/10643389.2021.1877976.

Edgar, R. C. 2013 UPARSE: Highly accurate OTU sequences from microbial amplicon reads. *Nature Methods* **10**(10), 996. https://doi.org/10.1038/nmeth.2604.

Gao, F., Zhou, X., Ma, Y., Zhang, X., Rong, X., Xiao, X., Wu, Z. & Wei, J. 2021 Calcium modified basalt fiber bio-carrier for wastewater treatment: Investigation on bacterial community and nitrogen removal enhancement of bio-nest. *Bioresource Technology* **335**. https://doi.org/10.1016/j.biortech.2021.125259.

Gao, Y., Zhang, Y., Wei, Q., Qi, X., Yin, Q., Liu, B. & He, K. 2023 Response and synergistic effect of microbial community to submerged macrophyte in restoring urban black and smelly water bodies. *Journal of Water Process Engineering* **53**. https://doi.org/10.1016/j.jwpe.2023.103906.

Gong, B., Duan, K., Chen, S. & Wang, Y. 2023 Enhanced nutrients removal and microbial mechanisms in a pilot-scale anaerobic-oxic-anoxic (A/O/A) system: Synergistic roles of denitrifying polyphosphate accumulating organisms and endogenous denitrifiers. *Process Safety and Environmental Protection* **179**, 47–56. https://doi.org/10.1016/j.psep.2023.08.085.

HACH, 2016 Water Analysis Handbook, second ed, Chemical Industry Press, Beijing.

He, L., Wu, D.-X., Zhang, X.-Y. & Peng, L. 2023 The exposure dose of reclaimed water in daily life: A mini review. *Water Cycle* **4**, 120–126. https://doi.org/https://doi.org/10.1016/j.watcyc.2023.05.003.

Hoshino, T., Terahara, T., Tsuneda, S., Hirata, A. & Inamori, Y. 2005 Molecular analysis of microbial population transition associated with the start of denitrification in a wastewater treatment process. *Journal of Applied Microbiology* **99**(5), 1165–1175. https://doi.org/10.1111/j.1365-2672.2005.02698.x.

Kalia, S., Thakur, K., Celli, A., Kiechel, M. A. & Schauer, C. L. 2013 Surface modification of plant fibers using environment friendly methods for their application in polymer composites, textile industry and antimicrobial activities: A review. *Journal of Environmental Chemical Engineering* **1**(3), 97–112. https://doi.org/https://doi.org/10.1016/j.jece.2013.04.009.

Kim, L. H., Choi, E. & Stenstrom, M. K. 2003 Sediment characteristics, phosphorus types and phosphorus release rates between river and lake sediments. *Chemosphere* **50**(1), 53–61. https://doi.org/10.1016/s0045-6535(02)00310-7.

Kim, B.-R., Shin, J., Guevarra, R. B., Lee, J. H., Kim, D. W., Seol, K.-H., Lee, J.-H., Kim, H. B. & Isaacson, R. E. 2017 Deciphering diversity indices for a better understanding of microbial communities. *Journal of Microbiology and Biotechnology* **27**(12), 2089–2093. https://doi.org/10.4014/jmb.1709.09027.

Leyva-Diaz, J. C., Monteoliva-Garcia, A., Martin-Pascual, J., Munio, M. M., Garcia-Mesa, J. J. & Poyatos, J. M. 2020 Moving bed biofilm reactor as an alternative wastewater treatment process for nutrient removal and recovery in the circular economy model. *Bioresource Technology* **299**. https://doi.org/10.1016/j.biortech.2019.122631.

Li, X., Yuan, Y. & Huang, Y. 2021 Enhancing the nitrogen removal efficiency of a new autotrophic biological nitrogen-removal process based on the iron cycle: Feasibility, progress, and existing problems. *Journal of Cleaner Production* **317**. https://doi.org/10.1016/j.jclepro.2021.128499.

Liu, A.-C., Chou, C.-Y., Chen, L.-L. & Kuo, C.-H. 2015 Bacterial community dynamics in a swine wastewater anaerobic reactor revealed by 16S rDNA sequence analysis. *Journal of Biotechnology* **194**, 124–131. https://doi.org/10.1016/j.jbiotec.2014.11.026.

Liu, J., Yang, J., Chen, M., Lei, L. & Wu, Z. 2018 Effect of SiO_2, Al_2O_3 on heat resistance of basalt fiber. *Thermochimica Acta* **660**, 56–60. https://doi.org/10.1016/j.tca.2017.12.023.

Liu, X., Xu, J., Huang, J., Huang, M., Wang, T., Bao, S., Tang, W. & Fang, T. 2019 Bacteria-supported iron scraps for the removal of nitrate from low carbon-to-nitrogen ratio wastewater. *RSC Advances* **9**(6), 3285–3293. https://doi.org/10.1039/c8ra09091b.

Lu, H.-P., Shao, Y.-H., Wu, J.-H. & Hsieh, C.-H. 2020 System performance corresponding to bacterial community succession after a disturbance in an autotrophic nitrogen removal bioreactor. *mSystems* **5**(4). https://doi.org/10.1128/msystems.00398-20.

Mariane de Morais, A. P., Abreu, P. C., Wasielesky, W. & Krummenauer, D. 2020 Effect of aeration intensity on the biofilm nitrification process during the production of the white shrimp *Litopenaeus vannamei* (Boone, 1931) in biofloc and clear water systems. *Aquaculture* **514**. https://doi.org/10.1016/j.aquaculture.2019.734516.

Nemeth, A., Ainsworth, J., Ravishankar, H., Lens, P. N. L. & Heffernan, B. 2023 Temperature dependence of nitrification in a membrane-aerated biofilm reactor. *Frontiers in Microbiology* **14**. https://doi.org/10.3389/fmicb.2023.1114647.

Ni, H., Zhou, X., Zhang, X., Xiao, X., Liu, J.F., Huan, H., Luo, Z. & Wu, Z. 2018 Feasibility of using basalt fiber as biofilm carrier to construct bio-nest for wastewater treatment. *Chemosphere* **212**, 768–776. https://doi.org/10.1016/j.chemosphere.2018.08.136.

Ni, H., Arslan, M., Qian, J., Wang, Y., Liu, Z., Luo, Z., Cai, R., Gamal El-Din, M. & Wu, Z. 2021 Application of basalt fibers in a biological contact oxidation reactor for the treatment of landfill leachate. *Journal of Cleaner Production* **297**. https://doi.org/10.1016/j.jclepro.2021.126648.

Ni, H., Wang, C., Arslan, M., Qian, J., Liang, Z., Luo, Z., Cai, R., Gamal El-Din, M. & Wu, Z. 2022 Enhanced wastewater treatment by modified basalt fiber bio-carriers: Effect of etching and surface functionalization. *Journal of Cleaner Production* **343**. https://doi.org/10.1016/j.jclepro.2022.130927.

Ni, H., Arslan, M., Zhang, T., Chen, L., Wang, Y., Qian, J., Cao, F., Wu, Z. & Gamal El-Din, M. 2023 Enhancing efficiency of biological contact oxidation reactors through filaments optimization of basalt fibers bio-carriers: Insights from a pilot-scale study. *Journal of Water Process Engineering* **55**. https://doi.org/10.1016/j.jwpe.2023.104134.

Niu, S., Gao, S., Zhang, K., Li, Z., Wang, G., Li, H., Xia, Y., Tian, J., Yu, E., Xie, J., Zhang, M. & Gong, W. 2023 Effects of hydraulic retention time and influent nitrate concentration on solid-phase denitrification system using wheat husk as carbon source. *PeerJ* **11**. https://doi.org/10.7717/peerj.15756.

Ouyang, W.-Y., Wang, W.-L., Zhang, Y.-L., Cai, H.-Y. & Wu, Q.-Y. 2023 VUV/UV oxidation performance for the elimination of recalcitrant aldehydes in water and its variation along the light-path. *Water Research* **228**, 119390. https://doi.org/https://doi.org/10.1016/j.watres.2022.119390.

Roche, K. R., Drummond, J. D., Boano, F., Packman, A. I., Battin, T. J. & Hunter, W. R. 2017 Benthic biofilm controls on fine particle dynamics in streams. *Water Resources Research* **53**(1), 222–236. https://doi.org/10.1002/2016wr019041.

Saini, S., Tewari, S., Dwivedi, J. & Sharma, V. 2023 Biofilm-mediated wastewater treatment: A comprehensive review. *Materials Advances* **4**(6), 1415–1443. https://doi.org/10.1039/d2ma00945e.

Shang, P., Dong, S., Han, Y., Bo, S., Ye, Y., Duan, M. & Chamba, Y. 2022 Environmental exposure to swine farms reshapes human gut microbiota. *Chemosphere* **307**, 135558. https://doi.org/https://doi.org/10.1016/j.chemosphere.2022.135558.

Siyu, W., Long, Y., Xiangchun, W. & Yuan, Z. 2021 Research advances of microbial denitrification and application in black and odorous water. *IOP Conference Series: Earth and Environmental Science* **825**, 012011. https://doi.org/10.1088/1755-1315/825/1/012011.

Tan, X., Yang, Y.-L., Liu, Y.-W., Li, X. & Zhu, W.-B. 2021 Quantitative ecology associations between heterotrophic nitrification-aerobic denitrification, nitrogen-metabolism genes, and key bacteria in a tidal flow constructed wetland. *Bioresource Technology* **337**. https://doi.org/10.1016/j.biortech.2021.125449.

Thuy, V. K., He, K., Echigo, S., Asada, Y. & Itoh, S. 2022 Impact of biological clogging and pretreatments on the operation of soil aquifer treatments for wastewater reclamation. *Water Cycle* **3**, 35–43. https://doi.org/https://doi.org/10.1016/j.watcyc.2022.03.001.

Tian, T. & Yu, H.-Q. 2020 Denitrification with non-organic electron donor for treating low C/N ratio wastewaters. *Bioresource Technology* **299**. https://doi.org/10.1016/j.biortech.2019.122686.

Tu, R., Jin, W., Han, S.-F., Zhou, X., Wang, T., Gao, S.-H., Wang, Q., Chen, C., Xie, G.-J. & Wang, Q. 2019 Rapid enrichment and ammonia oxidation performance of ammonia-oxidizing archaea from an urban polluted river of China. *Environmental Pollution* **255**. https://doi.org/10.1016/j.envpol.2019.113258.

Xia, J., Chundu, W., Zhiren, W. & Bo, Z. 2015 Basic characteristics and application of basalt fiber in the water pollution control. *Advanced Materials Research* **1073–1076**, 838–843. https://doi.org/10.4028/www.scientific.net/AMR.1073-1076.838.

Xuan, Y., Tang, C. & Cao, Y. 2020 Mechanisms of nitrate accumulation in highly urbanized rivers: Evidence from multi-isotopes in the Pearl River delta, China. *Journal of Hydrology* **587**. https://doi.org/10.1016/j.jhydrol.2020.124924.

Zhai, Q., Hong, Y., Wang, X., Wang, Q., Zhao, G., Liu, X. & Zhang, H. 2022 Mixing starch wastewaters to balance nutrients for improving nutrient removal, microalgae growth and accumulation of high value-added products. *Water Cycle* **3**, 151–159. https://doi.org/https://doi.org/10.1016/j.watcyc.2022.09.004.

Zhang, X., Zhou, X., Ni, H., Rong, X., Zhang, Q., Xiao, X., Huan, H., Liu, J.F. & Wu, Z. 2018 Surface modification of basalt fiber with organic/Inorganic composites for biofilm carrier used in wastewater treatment. *ACS Sustainable Chemistry & Engineering* **6**(2), 2596–2602. https://doi.org/10.1021/acssuschemeng.7b04089.

Zhang, X., Zhou, X., Xie, Y., Rong, X., Liu, Z., Xiao, X., Liang, Z., Jiang, S., Wei, J. & Wu, Z. 2019a A sustainable bio-carrier medium for wastewater treatment: Modified basalt fiber. *Journal of Cleaner Production* **225**, 472–480. https://doi.org/10.1016/j.jclepro.2019.03.333.

Zhang, X., Wei, J., Zhou, X., Horio, A., Li, S., Chen, Y., Jiang, S., Liang, Z., Wu, Z. & Qiu, F. 2019b Evaluation of modified basalt fiber as biological carrier media for wastewater treatment with the extended DLVO theory model. *Environmental Science and Pollution Research* **26**(29), 29789–29798. https://doi.org/10.1007/s11356-019-06133-7.

Zhang, H., Ma, B., Huang, T., Yang, W., Liu, X. & Niu, L. 2022 Nitrogen removal from low carbon/nitrogen polluted water is enhanced by a novel synthetic micro-ecosystem under aerobic conditions: Novel insight into abundance of denitrification genes and community interactions. *Bioresource Technology* **351**. https://doi.org/10.1016/j.biortech.2022.127013.

Zheng, L., Zhang, H., Li, C., Wu, Z., Yu, J., Xu, H., Chen, M. & Wei, Y. 2023 Roles of magnetic coagulation in black-odor water restoration: An insight into dissolved organic matters. *Water Cycle* **4**, 1–11. https://doi.org/https://doi.org/10.1016/j.watcyc.2022.11.002.

Zhou, X., Arslan, M., Liu, Z., Li, D., Xi, H., Feng, Y., Li, S., Wei, J., Rong, X., Liang, Z., Wang, X., Wu, Z. & El-Din, M. G. 2022 Low carbon-to-nitrogen ratio digestate from high-rate anaerobic baffled reactor facilitates heterotrophic/autotrophic nitrifiers involved in nitrogen removal. *Bioresource Technology* **359**. https://doi.org/10.1016/j.biortech.2022.127346.

First received 4 March 2024; accepted in revised form 12 July 2024. Available online 30 July 2024